

# Neutron diffraction study on magnetic structures and transitions in $\text{Sr}_2\text{Cr}_3\text{As}_2\text{O}_2$

Juanjuan Liu,<sup>1</sup> Jincheng Wang,<sup>1</sup> Jieming Sheng,<sup>1,2</sup> Feng Ye,<sup>2</sup> Keith M. Taddei,<sup>2</sup> J. A. Fernandez-Baca,<sup>2</sup> Wei Luo,<sup>3,1</sup> Guang-Ai Sun,<sup>3</sup> Zhi-Cheng Wang,<sup>4</sup> Hao Jiang,<sup>5</sup> Guang-Han Cao,<sup>4</sup> and Wei Bao<sup>1,\*</sup>

<sup>1</sup>*Department of Physics, Renmin University of China, Beijing 100872, China*

<sup>2</sup>*Neutron Scattering Division, Oak Ridge National Laboratory, Oak Ridge, Tennessee 37831, USA*

<sup>3</sup>*Key Laboratory of Neutron Physics, Institute of Nuclear Physics and Chemistry, China Academy of Engineering Physics, Mianyang 621999, China*

<sup>4</sup>*Department of Physics, Zhejiang University, Hangzhou 310027, China*

<sup>5</sup>*School of Physics and Optoelectronics, Xiangtan University, Xiangtan 411105, China*



(Received 26 March 2018; revised manuscript received 12 June 2018; published 10 October 2018)

$\text{Sr}_2\text{Cr}_3\text{As}_2\text{O}_2$  is composed of alternating square-lattice  $\text{CrO}_2$  and  $\text{Cr}_2\text{As}_2$  stacking layers, where  $\text{CrO}_2$  is isostructural to the  $\text{CuO}_2$  building-block of cuprate high- $T_c$  superconductors and  $\text{Cr}_2\text{As}_2$  to  $\text{Fe}_2\text{As}_2$  of Fe-based superconductors. Current interest in this material is raised by theoretic prediction of possible superconductivity. In this neutron powder diffraction study, we discovered that magnetic moments of Cr(II) ions in the  $\text{Cr}_2\text{As}_2$  sublattice develop a C-type antiferromagnetic structure below 590 K, and the moments of Cr(I) in the  $\text{CrO}_2$  sublattice form the  $\text{La}_2\text{CuO}_4$ -like antiferromagnetic order below 291 K. The staggered magnetic moment  $2.19(4) \mu_B/\text{Cr(II)}$  in the more itinerant  $\text{Cr}_2\text{As}_2$  layer is smaller than  $3.10(6) \mu_B/\text{Cr(I)}$  in the more localized  $\text{CrO}_2$  layer. Different from previous expectations, a spin-flop transition of the Cr(II) magnetic order observed at 291 K indicates a strong coupling between the  $\text{CrO}_2$  and  $\text{Cr}_2\text{As}_2$  magnetic subsystems.

DOI: [10.1103/PhysRevB.98.134416](https://doi.org/10.1103/PhysRevB.98.134416)

## I. INTRODUCTION

It is well known that the square-lattice  $\text{CuO}_2$  layer is the essential building block of cuprate superconductors [1]. The antiferromagnetic order in the  $\text{CuO}_2$  layer is suppressed by charge doping which gives rise to high-temperature superconductivity [2]. For the more recently discovered iron pnictide superconductors, the common structural ingredient is the  $\text{Fe}_2\text{As}_2$  layer [3], and the interplay between antiferromagnetism in the layer and superconductivity has attracted intense research interest [4–7]. The fact that unconventional superconductivity with high transition temperature ( $T_c$ ) tends to occur in materials containing the  $\text{CuO}_2$  or  $\text{Fe}_2\text{As}_2$  structural ingredient has inspired investigation on materials of the same structural building blocks. A new type of unconventional superconductivity was discovered in  $\text{Sr}_2\text{RuO}_4$  [8] and the stripe physics, a correlated charge, and antiferromagnetic order phenomenon was uncovered in  $\text{Sr}_2\text{NiO}_4$  [9] when Cu in the cuprate  $\text{Sr}_2\text{CuO}_4$  was replaced by Ru or Ni. Superconductivity has also been discovered in doped  $\text{CoO}_2$  layered compounds [10]. Similarly, isostructural materials of the iron pnictide superconductors have also been the focus of recent research. It has been proposed in theoretic studies that superconductivity could be induced by electron doping  $\text{LaCrAsO}$  [11,12] and  $\text{BaCr}_2\text{As}_2$  [13], similar to the “1111” and “122”-type Fe-based superconductors [3,14]. Experimental studies have been carried out so far on the parent compounds  $\text{LaCrAsO}$  [15],  $\text{BaCr}_2\text{As}_2$  [16],  $\text{SrCr}_2\text{As}_2$  [17], and  $\text{EuCr}_2\text{As}_2$  [18], and these materials are found to be metallic, and to develop a G-type

antiferromagnetic order with the Néel temperature as high as 600 K.

An interesting family of oxipnictides  $A_2\text{Mn}_3\text{Pn}_2\text{O}_2$  ( $A = \text{Sr, Ba}$  and  $\text{Pn} = \text{P, As, Sb, Bi}$ ) [19–28] is formed of alternating  $\text{CuO}_2$ -type and  $\text{Fe}_2\text{As}_2$ -type layers, containing the key structural ingredients of both the cuprate and Fe-based superconductors. The two different types of Mn square lattices of  $\text{MnO}_2$  and  $\text{Mn}_2\text{As}_2$  stacking along the  $c$  axis with the tetragonal space group  $I4/mmm$  (No. 139). The isostructural “2322” oxysulfides also exist [29–34]. Although  $A_2\text{Mn}_3\text{Pn}_2\text{O}_2$  are antiferromagnetic insulators, it was suggested in theoretic works that superconductivity can be realized in the 2322 family with a proper choice of the transition metal to substitute Mn [35–37]. Motivated by the theoretic suggestion, the chromium-based 2322 material  $\text{Sr}_2\text{Cr}_3\text{As}_2\text{O}_2$  was recently synthesized [38], containing alternating  $\text{CrO}_2$  and  $\text{Cr}_2\text{As}_2$  layers along the  $c$  axis, see Fig. 1(a). The electrical resistivity shows metallic response [38], as in the recently investigated 1111 and 122-type chromium pnictides [15–18].

In  $A_2\text{Mn}_3\text{Pn}_2\text{O}_2$ , the  $\text{Mn}_2\text{Pn}_2$  layer tends to form a G-type antiferromagnetic order around 300 K [23]. The magnetic couplings in the  $\text{MnO}_2$  layer are significantly weaker. While the  $\text{MnO}_2$  layer in  $\text{Sr}_2\text{Mn}_3\text{Sb}_2\text{O}_2$  forms long-range magnetic order at 65 K [23], it shows only short-range magnetic order with a spin freezing behavior below  $\sim 50$  K in compounds such as  $\text{Sr}_2\text{Mn}_3\text{As}_2\text{O}_2$  [23],  $\text{Sr}_2\text{Zn}_2\text{As}_2\text{MnO}_2$  [26], and  $\text{Ba}_2\text{Zn}_2\text{As}_2\text{MnO}_2$  [27].

For  $\text{Sr}_2\text{Cr}_3\text{As}_2\text{O}_2$ , anomalies in electric resistivity, magnetic susceptibility and heat capacity were observed below the room temperature, indicating magnetic transitions in line with the prediction of magnetically ordered ground state in both the  $\text{CrO}_2$  and  $\text{Cr}_2\text{As}_2$  layers from first principle

\*wbao@ruc.edu.cn

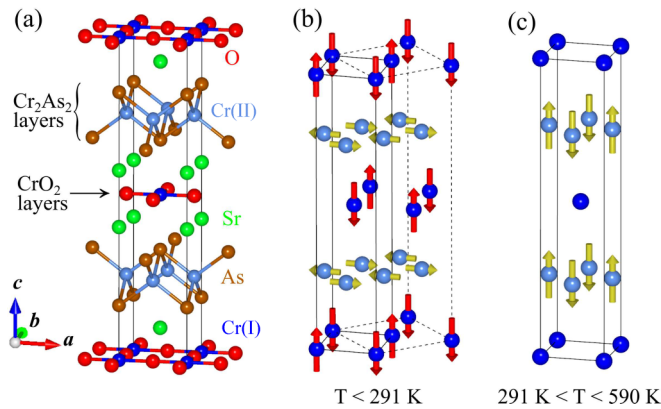


FIG. 1. (a) Crystal structure of  $\text{Sr}_2\text{Cr}_3\text{As}_2\text{O}_2$ . The atoms are noted by different colors. Layers of  $\text{CrO}_2$  squares and  $\text{Cr}_2\text{As}_2$  tetrahedra are labeled. (b) The magnetic structure below 291 K when both  $\text{CrO}_2$  layer and  $\text{Cr}_2\text{As}_2$  layer order. (c) The magnetic structure above 291 K when only the  $\text{Cr}_2\text{As}_2$  layer orders. The solid lines in (b) and (c) are the structural unit cell identical to the cell in (a), and the dash lines in (b) are the magnetic unit cell with  $a_{\text{mag}} = a + b$ ,  $b_{\text{mag}} = a - b$ .

calculation [38]. However, the nature of magnetic transitions at the bulk measurement anomalies remains unclear. Therefore, we have conducted a neutron powder diffraction study on  $\text{Sr}_2\text{Cr}_3\text{As}_2\text{O}_2$  to investigate magnetic structures in the two Cr sublattices and the corresponding phase transitions.

We found that the magnetic moments of the Cr(II) ions in the  $\text{Cr}_2\text{As}_2$  sublattice develop a C-type antiferromagnetic order at a temperature as high as 590 K with the  $c$  axis as the magnetic easy axis, see Fig. 1(c). The in-plane magnetic arrangement of  $\text{Sr}_2\text{Cr}_3\text{As}_2\text{O}_2$  is the same as in the G-type antiferromagnetic order of the 1111 and 122-type chromium pnictides [15–18]; however, the interplane Cr(II) ions are ferromagnetically (FM) aligned in contrast to the case in the G-type order in those chromium pnictides. Below 291 K, the Cr(I) ions in the  $\text{CrO}_2$  sublattice form a  $\text{K}_2\text{NiF}_4$ -type [39] long-range antiferromagnetic order with moments along the  $c$  direction, see Fig. 1(b). This is the same antiferromagnetic order discovered in the cuprate  $\text{La}_2\text{CuO}_4$  [40]. When the Cr(I) sublattice orders at 291 K, a spin-flop transition occurs on the Cr(II) sublattice with the moment direction flips from the  $c$  axis to the  $ab$  plane. The observed magnetic structure is different from the prediction from the first-principle calculations [38].

## II. EXPERIMENTAL METHODS

The polycrystalline sample of  $\text{Sr}_2\text{Cr}_3\text{As}_2\text{O}_2$  was grown by solid-state reactions using SrO (99.5%), Cr (99.9%), and As (99.999%) as starting materials [38]. The sample was initially examined using the high-resolution neutron powder diffractometer at the Key Laboratory of Neutron Physics, China Academy of Engineering Physics (CAEP). Neutron powder diffraction measurements were carried out on the HB-2A neutron powder diffractometer [41] at the High Flux Isotope Reactor (HFIR), Oak Ridge National Laboratory. On HB-2A, neutron wavelength of  $\lambda = 2.4101 \text{ \AA}$  and  $1.5392 \text{ \AA}$  were selected by the vertically focused Ge(113) and Ge(115)

monochromator, respectively. The beam was collimated by the 21' Soller collimator before sample and 12' before detectors. Approximate 5.74 g powder sample was sealed in a cylindrical Al container with helium as exchange gas to ensure thermal equilibrium. It was loaded into a closed cycle refrigerator that regulates the temperature from 4 K to 300 K. High temperature neutron data were taken on the HB-1A triple-axis spectrometer at HFIR with fixed incident neutron energy 14.64 meV (wavelength 2.364  $\text{\AA}$ ) produced by the double pyrolytic graphite monochromator system. The temperature was regulated by high temperature Displex from 30 K to 700 K.

In addition to the main phase of  $\text{Sr}_2\text{Cr}_3\text{As}_2\text{O}_2$ , an unidentified minor impurity phase and the Al sample environment also contribute to the neutron diffraction spectra collected. From the temperature independence of the neutron-diffraction impurity Bragg peaks and additional x-ray diffraction measurements of the impurity peaks, the impurity phase is concluded to contain no magnetic neutron diffraction contribution. Using FullProf Suite package [42], the Al peaks are accounted by Le Bail fitting [44], the minority contributions are isolated, and the nuclear and magnetic structures of the main phase were refined using the Rietveld method [43]. The Thompson-Cox-Hastings pseudo-Voigt function corrected by axial divergence asymmetry was used to model the peak profiles of all phases. Due to the existence of the Al and impurity peaks, the overall thermal factor for all atoms is used at each temperature, since the refinement of the thermal factor for each individual atom is unreliable in this case. BasIreps program of FullProf Suite is used for representation analysis to derive the possible magnetic structure modes.

## III. RESULTS AND DISCUSSIONS

The neutron powder diffraction pattern measured at room temperature is shown in Fig. 2. At 300 K, two wavelengths were used, as the shorter wavelength of neutron probes the structure in a larger reciprocal-space range. The refined parameters from various measurements are summarized in Table I. The number in parentheses is the standard deviation from the Rietveld refinement. Its high precision reflects the high self-consistency of the spectra measured using the high-flux and high-resolution modern neutron diffractometer, and the difference in the two sets of the 300 K refinement parameters represents the systematic error from the two different measurement setups, as discussed previously in literature [45,46]. Consistent with earlier reports [38],  $\text{Sr}_2\text{Cr}_3\text{As}_2\text{O}_2$  crystallizes in the tetragonal space group  $I4/mmm$  (No. 139). The Cr(I) in the  $\text{CrO}_2$  layer resides at the Wyckoff 2a site, and forms a body-centered sublattice. The Cr(II) in the  $\text{Cr}_2\text{As}_2$  layer resides at the Wyckoff 4d site, and forms a primitive sublattice.

Both the As-M-As bond angle (M denotes transition metal) and the As height are important parameters controlling the electronic states driven by the  $p-d$  hybridization and exchange interactions. In the iron-based superconductors, the As-Fe-As bond angle and the anion height were found in close relation to superconducting transition temperatures  $T_c$ . To achieve optimal  $T_c$ , it was suggested to have regular  $\text{FeAs}_4$  tetragonal with the As-Fe-As bond angle close to  $109.47^\circ$

TABLE I. The Rietveld refinement results of  $\text{Sr}_2\text{Cr}_3\text{As}_2\text{O}_{12}$  from the neutron powder diffraction data at various temperatures and wavelengths. The atomic positions are Sr (0,0, $z_{\text{Sr}}$ ) in Wyckoff 4e site, Cr(I) (0,0,0) in 2a site, Cr(II) (0,0.5,0.25) in 4d site, As (0,0, $z_{\text{As}}$ ) in 4e site, and O (0,0.5,0) in 4c site. The twofold and fourfold multiplicities of As-Cr(II)-As angles are denoted.

T (K)	300	300	260	230	200	100	4
wavelength (Å)	1.5392	2.4101	2.4101	2.4101	2.4101	2.4101	2.4101
$a$ (Å)	4.00671(6)	4.00574(5)	4.00417(6)	4.00306(6)	4.00198(6)	3.99941(6)	3.99892(6)
$c$ (Å)	18.8310(5)	18.8261(5)	18.8029(5)	18.7862(5)	18.7717(5)	18.7303(5)	18.7151(5)
$V$ (Å <sup>3</sup> )	302.31(1)	302.08(1)	301.47(1)	301.04(1)	300.64(1)	299.60(1)	299.28(1)
$z_{\text{Sr}}$	0.4125(2)	0.4117(2)	0.4120(2)	0.4128(2)	0.4123(2)	0.4115(2)	0.4113(2)
$z_{\text{As}}$	0.8298(2)	0.8308(2)	0.8305(2)	0.8304(2)	0.8304(2)	0.8309(2)	0.8308(2)
$B$ (Å <sup>2</sup> )	0.77(2)	0.60(4)	0.47(4)	0.42(4)	0.34(4)	0.30(4)	0.18(4)
As height (Å)	1.503(3)	1.521(4)	1.514(4)	1.510(4)	1.510(4)	1.515(4)	1.512(4)
As-Cr(II)-As angle (deg) $\times 2$	106.23(6)	105.57(7)	105.82(7)	105.92(7)	105.95(7)	105.69(7)	105.80(7)
As-Cr(II)-As angle (deg) $\times 4$	111.1(1)	111.5(2)	111.3(2)	111.3(2)	111.3(2)	111.4(2)	111.3(2)
$m$ ( $\mu_B/\text{Cr(II)}$ )	1.97(4)	1.97(3)	2.02(4)	2.11(4)	2.12(4)	2.18(4)	2.19(4)
$m$ ( $\mu_B/\text{Cr(I)}$ )	0	0	2.46(7)	2.69(7)	2.78(6)	3.07(6)	3.10(6)
$R_p$ (%)	4.01	3.94	4.04	4.36	4.07	4.24	4.48
$R_{\text{wp}}$ (%)	5.43	5.55	6.04	6.48	6.44	6.33	6.53

[47,48] or anion height close to 1.38 Å [49]. Here, the As-Cr(II)-As bond angle of  $\text{Sr}_2\text{Cr}_3\text{As}_2\text{O}_{12}$  is around 105.8° and 111.3°, and the As height is around 1.51 Å, with little temperature dependence from 300 K to 4 K as seen from Table I.

Three peaks indexed as (1,0,0), (1,0,2), and (1,0,4) that are forbidden by the crystal symmetry were observed at 300 K, as presented in the inset of Fig. 2(b). These intensities are accounted by the C-type magnetic structure of the Cr(II) spins in the  $\text{Cr}_2\text{As}_2$  layer shown in Fig. 1(c). It is antiferromagnetically (AFM) arranged for intralayer nearest-neighbor spins but FM arranged for interlayer spins, resulting in wave-vector (1,0,0). The moment direction is along the  $c$  axis, and the moment size is 1.97(4)  $\mu_B/\text{Cr(II)}$  at 300 K. The magnetic structure persists

up as high as 590.3(7) K, as demonstrated by the temperature dependence of (1,0,0) peak in Fig. 3(a).

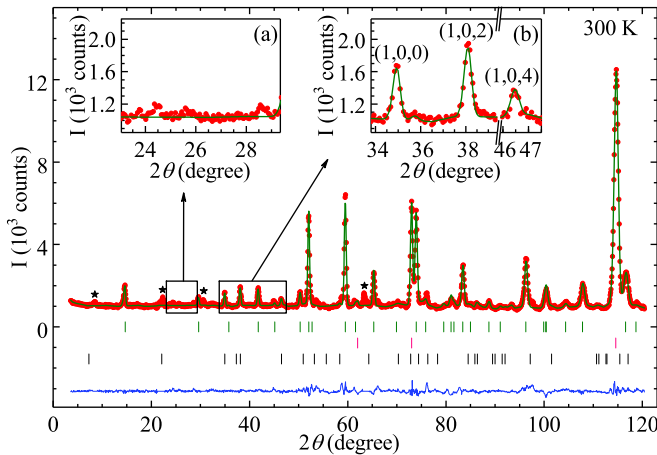


FIG. 2. The neutron diffraction pattern of  $\text{Sr}_2\text{Cr}_3\text{As}_2\text{O}_{12}$  at room temperature, with wavelength  $\lambda = 2.4101$  Å. The observation, calculation, and their difference are denoted in red circles, green and blue lines, respectively. The vertical bars in green, red, and black mark the nuclear Bragg peak positions of  $\text{Sr}_2\text{Cr}_3\text{As}_2\text{O}_{12}$ , Al, and magnetic Bragg peak positions from the Cr(II) sublattice. The impurity peaks are marked with stars and are excluded during refinement. The inset (a) zooms in expected positions of magnetic peaks of wave-vector  $(\frac{1}{2}, \frac{1}{2}, 0)$  and inset (b) magnetic peaks of wave-vector (1,0,0).

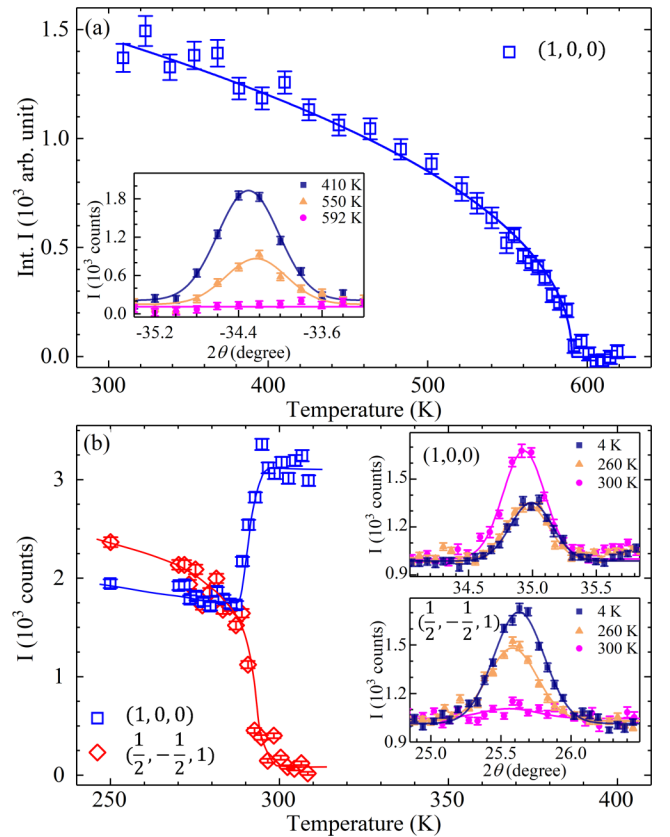


FIG. 3. (a) Temperature dependence of the integrated intensity of the magnetic Bragg peak (1,0,0). The solid line and onset temperature of  $T_N = 590.3(7)$  K was obtained by fitting to the order parameter function  $I/I_0 = (1 - \frac{T}{T_N})^{2\beta} + b_0$ . (b) Temperature dependence of the background corrected peak intensity of the Bragg peaks (1,0,0) and  $(\frac{1}{2}, -\frac{1}{2}, 1)$ . The solid lines are guides to eyes. The insets are the peaks profiles for (1,0,0) and  $(\frac{1}{2}, -\frac{1}{2}, 1)$  at selected temperatures.

The high ordering temperature and the intralayer AFM pattern established in the  $\text{Cr}_2\text{As}_2$  layer of  $\text{Sr}_2\text{Cr}_3\text{As}_2\text{O}_2$  resemble those in other chromium pnictides. In 1111-type  $\text{LaCrAsO}$  [15], and the 122-type  $\text{BaCr}_2\text{As}_2$ ,  $\text{SrCr}_2\text{As}_2$ , and  $\text{EuCr}_2\text{As}_2$  [16–18], the same intralayer spin arrangement and ordering temperature around 600 K were found. This reveals a robust AFM intralayer coupling which does not change across compositions. However, in  $\text{Sr}_2\text{Cr}_3\text{As}_2\text{O}_2$  the inter-layer coupling becomes FM, in contrast to the 1111 and 122 chromium pnictides which have AFM interlayer couplings in the G-type magnetic structure.

Below 291 K, new peaks appear that can be indexed by the wave-vector  $\mathbf{k}' = (\frac{1}{2}, \frac{1}{2}, 0)$ , while the  $\mathbf{k}'' = (1, 0, 0)$  type of peaks change their relative intensities, e.g., the  $(1, 0, 0)$  and  $(1, 0, 2)$  peaks are reduced and the  $(1, 0, 4)$  peak is enhanced. This is demonstrated in Fig. 3(b) by abrupt changes of magnetic peaks intensities on  $(1, 0, 0)$  and  $(\frac{1}{2}, -\frac{1}{2}, 1)$  around 291 K. As we will demonstrate, the arise of  $(\frac{1}{2}, \frac{1}{2}, 0)$  series of peaks corresponds to the magnetic order established on the Cr(I) sublattice in the  $\text{CrO}_2$  layer, and the intensity change of the  $(1, 0, 0)$ ,  $(1, 0, 2)$ ,  $(1, 0, 4)$ , etc. Bragg peaks corresponds to a sudden flip of Cr(II) moment in the  $\text{Cr}_2\text{As}_2$  layer. The transition is responsible for the susceptibility anomaly observed around 291 K [38]. The first-order-like transitions in both the  $(\frac{1}{2}, \frac{1}{2}, 0)$  and  $(1, 0, 0)$  type magnetic Bragg peaks [Fig. 3(b)] suggest strong interaction between the Cr(I) and Cr(II) ions.

Magnetic Bragg peaks below 291 K are fitted by the magnetic structure depicted in Fig. 1(b), with the Cr(I) and Cr(II) moment sizes the only two refined parameters. The magnetic order on the Cr(I) site of the  $\text{CrO}_2$  layer is responsible for the  $(\frac{1}{2}, \frac{1}{2}, 0)$  wave vector. The nearest neighbors of intralayer Cr(I) spins are AFM aligned, and the moments point to  $c$  axis. The magnetic structure of the body-centered Cr(I) sublattice mimics that of the body-centered  $\text{K}_2\text{NiF}_4$  [39]. Interestingly, when the Cr(I) sublattice orders, the moments at the Cr(II) site in the  $\text{Cr}_2\text{As}_2$  layer flip into the  $ab$  plane. The magnetic structure where two sublattices have orthogonal spin orientations persists down to 4 K, the base temperature in our measurement. The diffraction pattern together with the fits at 4 K are presented in Fig. 4. In principle, the specific in-plane moment direction of tetragonal structure cannot be resolved from powder diffraction data due to the powder-averaged intensity [50]. We therefore don't distinguish the in-plane moment direction of Cr(II), and the Cr(II) moment direction in Fig. 1(b) is plotted for illustration purposes. The refined moments on the Cr(I) and Cr(II) sublattices at each temperatures are summarized in Table I. From 300 K to 260 K, a quick increase of Cr(I) moment size is witnessed when the order is established. This is then followed by a slower increase rate and gradual saturation down to the base temperature. For the Cr(II) moments, despite an abrupt change of the direction, the ordered moment of Cr(II) shows very small change below 300 K.

The magnetic structures above and below 291 K are further confirmed by the representation analysis [51]. The space group for the crystal structure is  $I4/mmm$ . For wave-vector  $\mathbf{k}' = (\frac{1}{2}, \frac{1}{2}, 0)$ , the little group  $mmm$  that leaves the wave vector unchanged has eight one-dimensional irreducible representations (IR)  $\Gamma'_1 \dots \Gamma'_8$ . The linear spaces spanned by spin

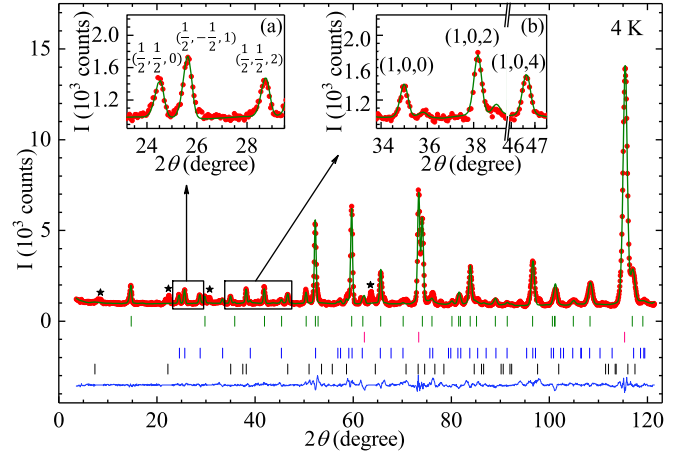


FIG. 4. The observed and calculated neutron diffraction pattern of  $\text{Sr}_2\text{Cr}_3\text{As}_2\text{O}_2$  at  $T = 4$  K, with wavelength  $\lambda = 2.4101$  Å. The observation, calculation, and their difference are denoted in red circles, green and blue lines, respectively. The vertical bars in green and red mark the nuclear Bragg peaks positions of  $\text{Sr}_2\text{Cr}_3\text{As}_2\text{O}_2$  and Al, respectively. The vertical bars in blue and black mark the magnetic Bragg peaks positions from the Cr(I) and Cr(II) sublattice, respectively. The impurity peaks are marked with stars and are excluded during refinement. The inset (a) zooms in magnetic peaks of wave-vector  $(\frac{1}{2}, \frac{1}{2}, 0)$  and inset (b) magnetic peaks of wave-vector  $(1, 0, 0)$ .

vectors on site Cr(I) and Cr(II) are three dimensional and six dimensional, respectively. Therefore, they can be decomposed to three and six one-dimensional IRs of group  $mmm$

$$\Gamma'_{\text{Cr(I)}} = 1\Gamma'_3 + 1\Gamma'_5 + 1\Gamma'_7,$$

and

$$\Gamma'_{\text{Cr(II)}} = 1\Gamma'_1 + 1\Gamma'_2 + 1\Gamma'_3 + 1\Gamma'_4 + 1\Gamma'_7 + 1\Gamma'_8.$$

Only the magnetic structure of  $\Gamma'_3$  for Cr(I) spins fits the magnetic Bragg peaks of  $(\frac{1}{2}, \frac{1}{2}, 0)$  series. For wave-vector  $\mathbf{k}'' = (1, 0, 0)$ , the little group is the same as the crystal point group  $4/mmm$ . It has eight one-dimensional IRs  $\Gamma''_1 \dots \Gamma''_8$  and two two-dimensional IRs  $\Gamma''_9$  and  $\Gamma''_{10}$ . The spin spaces on site Cr(I) and Cr(II) can be decomposed as

$$\Gamma''_{\text{Cr(I)}} = 1\Gamma''_7 + 1\Gamma''_{10},$$

and

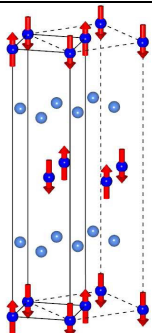
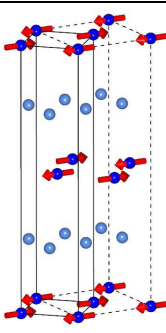
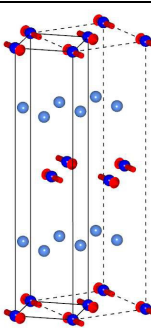
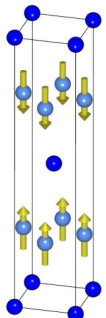
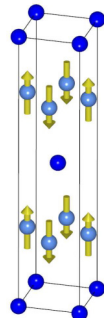
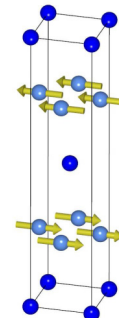
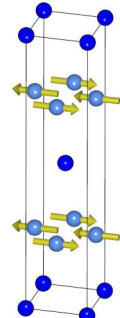
$$\Gamma''_{\text{Cr(II)}} = 1\Gamma''_2 + 1\Gamma''_5 + 1\Gamma''_9 + 1\Gamma''_{10}.$$

The magnetic Bragg peaks of  $(1, 0, 0)$  series above 291 K come from the  $\Gamma''_5$  of Cr(II) spins, and below 291 K the  $\Gamma''_{10}$  of Cr(II) spins. The three decomposed IRs of Cr(I) spins with wave-vector  $(\frac{1}{2}, \frac{1}{2}, 0)$  and four IRs of Cr(II) spins with wave-vector  $(1, 0, 0)$  are illustrated in Table II.

The magnetic structure of  $\text{Sr}_2\text{Cr}_3\text{As}_2\text{O}_2$  makes interesting comparison to other 2322 compounds such as the manganese analog  $\text{A}_2\text{Mn}_3\text{Pn}_2\text{O}_2$  and chromium pnictides  $\text{LaCrAsO}$  and  $\text{BaCr}_2\text{As}_2$ . In  $\text{A}_2\text{Mn}_3\text{Pn}_2\text{O}_2$  and chromium pnictides, the magnetic moments in the  $\text{Mn}_2\text{As}_2$  and  $\text{Cr}_2\text{As}_2$  sublattices form AFM arrangement both within and between layers with the wave-vector  $(1, 0, 1)$  in the so-called G-type magnetic



TABLE II. The basis vectors (BV) of decomposed irreducible representations (IR) of space group  $I4/mmm$  (No. 139) with wave-vector  $(\frac{1}{2}, \frac{1}{2}, 0)$  and moments on  $2a$  site (Cr(I) in  $\text{CrO}_2$  layer), as well as wave-vector  $(1, 0, 0)$  and moments on  $4d$  site (Cr(II) in  $\text{Cr}_2\text{As}_2$  layer). The corresponding magnetic structures are displayed. The solid line depicts the crystallographic unit cell, while the dashed line depicts the magnetic cell.

		Cr(I) at $2a$ site, $\mathbf{k}' = (\frac{1}{2}, \frac{1}{2}, 0)$			
Irrep		$\Gamma'_3$	$\Gamma'_5$	$\Gamma'_7$	
BV for site $(0,0,0)$		$(0, 0, m_z)$	$(m_x, m_x, 0)$	$(m_x, -m_x, 0)$	
Magnetic structure					
		Cr(II) at $4d$ site, $\mathbf{k}'' = (1, 0, 0)$			
Irrep		$\Gamma''_2$	$\Gamma''_5$	$\Gamma''_9$	$\Gamma''_{10}$
BV for site $(0,0.5,0.25)$		$(0, 0, m_z)$	$(0, 0, m_z)$	$(m_x, 0, 0)$	$(0, m_y, 0)$
BV for site $(0,0.5,0.75)$		$(0, 0, -m_z)$	$(0, 0, m_z)$	$(-m_x, 0, 0)$	$(0, -m_y, 0)$
Magnetic structure					

structure [15,23,27,52]. In  $\text{Sr}_2\text{Cr}_3\text{As}_2\text{O}_2$ , however, the inter-layer spin arrangement is FM and the magnetic structure becomes a C-type with the magnetic wave-vector  $(1,0,0)$ . The magnetic  $\text{CrO}_2$  buffer layer between the  $\text{Cr}_2\text{As}_2$  layers might be responsible for the change of the coupling sign. The ordering temperatures for the  $\text{Mn}_2\text{As}_2$  sublattice in  $\text{A}_2\text{Mn}_3\text{Pn}_2\text{O}_2$  are around 300 K. But for the  $\text{Cr}_2\text{As}_2$  sublattice in chromium pnictides and  $\text{Sr}_2\text{Cr}_3\text{As}_2\text{O}_2$ , the ordering temperatures are close to 600 K, indicating much stronger interaction strength in the  $\text{Cr}_2\text{As}_2$  sublattice than the  $\text{Mn}_2\text{As}_2$  sublattice.

The  $\text{MnO}_2$  layers in  $\text{Sr}_2\text{Mn}_3\text{Sb}_2\text{O}_2$ ,  $\text{Sr}_2\text{Mn}_3\text{As}_2\text{O}_2$  and  $\text{Ba}_2\text{Zn}_2\text{MnAs}_2\text{O}_2$  establish magnetic order with wave-vector  $(\frac{1}{2}, \frac{1}{2}, 0)$  [23,26,27], the same as the  $\text{CrO}_2$  layer in  $\text{Sr}_2\text{Cr}_3\text{As}_2\text{O}_2$ . However, only in  $\text{Sr}_2\text{Mn}_3\text{Sb}_2\text{O}_2$  the magnetic order is long-ranged and at a much reduced temperature of 65 K. In  $\text{Sr}_2\text{Mn}_3\text{As}_2\text{O}_2$ ,  $\text{Sr}_2\text{Zn}_2\text{MnAs}_2\text{O}_2$  and  $\text{Ba}_2\text{Zn}_2\text{MnAs}_2\text{O}_2$ , the magnetic order is short-ranged with a spin freezing behavior. These contrast to the long-range order at 291 K for the  $\text{CrO}_2$  layer spins in  $\text{Sr}_2\text{Cr}_3\text{As}_2\text{O}_2$ . Again the magnetic interactions in the  $\text{CrO}_2$  sublattice of  $\text{Sr}_2\text{Cr}_3\text{As}_2\text{O}_2$

are much stronger than in the  $\text{MnO}_2$  sublattice in  $\text{A}_2\text{Mn}_3\text{Pn}_2\text{O}_2$ .

The moments in the  $\text{Cr}_2\text{As}_2$  layer are along the  $c$  direction above 291 K, consistent with the orientation in the 1111 and 122 chromium pnictides. This reflects the same easy axis due to the single-ion anisotropy of  $\text{Cr}^{2+}$  in the  $\text{Cr}_2\text{As}_2$  environment. However, the magnetic ordering of the Cr(I) ions along the  $c$  direction in the  $\text{CrO}_2$  sublattice flips the Cr(II) ions in the  $\text{Cr}_2\text{As}_2$  sublattice into the  $ab$  plane, changing the easy axis in the  $\text{Cr}_2\text{As}_2$  layer. The magnetic structure where two sublattices have orthogonal moment directions was also observed in  $\text{Sr}_2\text{Mn}_3\text{Sb}_2\text{O}_2$  [23], although in a reverse way: the moments in the  $\text{Mn}_2\text{As}_2$  layer order along the  $c$  direction, and in the  $\text{MnO}_2$  layer in the  $ab$  plane. It was believed previously that in the 2322 compounds the two sublattices show independent magnetic behaviors and the interaction between the two sublattices was negligible [23]. The abrupt spin-flop transition found in our work on  $\text{Sr}_2\text{Cr}_3\text{As}_2\text{O}_2$  [Fig. 3(b)] provides evidence that the two magnetic sublattices are closely correlated. The magnetic state of orthogonal moment directions in the two

sublattices was not reproduced through simple bilayer classical spin model with experimentally achievable interactions strengths [53]. The nature of interaction and origin for the orthogonal spin orientation thus deserve more investigations.

While  $A_2Mn_3Pn_2O_2$  are insulators,  $Sr_2Cr_3As_2O_2$  and other chromium pnictides are metallic. We noticed that the conduction electrons are mostly from the  $Cr_2As_2$  layer, while electrons of the  $CrO_2$  layer are largely localized in the first principle calculations [38]. The saturation moment is  $2.2 \mu_B$  per Cr(II) in the  $Cr_2As_2$  layer and  $3.1 \mu_B$  per Cr(I) in the  $CrO_2$  layer. There is a larger reduction of the saturated moment in the itinerant  $Cr_2As_2$  layer than in the localized  $CrO_2$  layer from the  $4 \mu_B$  per  $Cr^{2+}$  ion in the  $3d^4$  high spin state. Therefore, it is tempted to state that the  $Cr_2As_2$  layer contributes itinerant moments and the  $CrO_2$  layer local moments, although it could be more complex due to correlations and interplay of itinerant and local electrons from two sublattices.

#### IV. CONCLUSION

We have performed neutron powder diffraction experiments from 4 to 620 K to investigate magnetic structures and magnetic transitions in  $Sr_2Cr_3As_2O_2$ . We discovered successive magnetic transitions in the material. The Cr(II) ions in the  $Cr_2As_2$  sublattice develop a C-type antiferromagnetic order of the magnetic wave-vector (1,0,0) at 590.3(7) K with the

magnetic easy axis along the  $c$  direction. Below 291 K, a  $K_2NiF_4$ -like antiferromagnetic order of the Cr(I) ions occurs with the magnetic wave-vector  $(\frac{1}{2}, \frac{1}{2}, 0)$  in the  $CrO_2$  sublattice with the easy  $c$  axis. At the same transition at 291 K, magnetic moments of the Cr(II) ions in the  $Cr_2As_2$  sublattice flip into the  $ab$  plane. The magnetic structure of orthogonal moment orientation in the two sublattices persists down to 4 K. The interplay between the two magnetic sublattices may play an important role in facilitating the spin-flop transition of Cr(II) moments.

#### ACKNOWLEDGMENTS

The work at RUC was supported by the National Basic Research Program of China (Grant No. 2012CB921700), the National Natural Science Foundation of China (Grant No. 11190024), and the Key Laboratory of Neutron Physics, CAEP (Grant No. 2017CB01). J.L. and J.W. acknowledge support from the Research Funds of RUC (Grant No. 17XNLF04 and 17XNLF06). J.S. acknowledges support from China Scholarship Council. The work at Z.U. was supported by the National Key Research and Development Program of China (No. 2017YFA0303002). Research at Oak Ridge National Laboratory was sponsored by the Scientific User Facilities Division, Office of Basic Energy Sciences, U.S. Department of Energy.

J.L. and J.W. contributed equally to this work.

- 
- [1] J. G. Bednorz and K. A. Müller, *Z. Phys. B* **64**, 189 (1986).
  - [2] P. A. Lee, N. Nagaosa, and X.-G. Wen, *Rev. Mod. Phys.* **78**, 17 (2006).
  - [3] Y. Kamihara, T. Watanabe, M. Hirano, and H. Hosono, *J. Am. Chem. Soc.* **130**, 3296 (2008).
  - [4] K. Ishida, Y. Nakai, and H. Hosono, *J. Phys. Soc. Jpn.* **78**, 062001 (2009).
  - [5] D. C. Johnston, *Adv. Phys.* **59**, 803 (2010).
  - [6] P. J. Hirschfeld, M. M. Korshunov, and I. I. Mazin, *Rep. Prog. Phys.* **74**, 124508 (2011).
  - [7] W. Bao, *Chin. Phys. B* **22**, 087405 (2013).
  - [8] A. Mackenzie and Y. Maeno, *Rev. Mod. Phys.* **75**, 657 (2003).
  - [9] J. M. Tranquada, P. Wochner, and D. J. Buttrey, *Phys. Rev. Lett.* **79**, 2133 (1997).
  - [10] K. Takada, H. Sakurai, E. Takayama-Muromachi, F. Izumi, R. A. Dilanian, and T. Sasaki, *Nature* **422**, 53 (2003).
  - [11] W.-S. Wang, M. Gao, Y. Yang, Y.-Y. Xiang, and Q.-H. Wang, *Phys. Rev. B* **95**, 144507 (2017).
  - [12] J. M. Pizarro, M. J. Calderón, J. Liu, M. C. Muñoz, and E. Bascones, *Phys. Rev. B* **95**, 075115 (2017).
  - [13] M. Edelmann, G. Sangiovanni, M. Capone, and L. de' Medici, *Phys. Rev. B* **95**, 205118 (2017).
  - [14] M. Rotter, M. Tegel, and D. Johrendt, *Phys. Rev. Lett.* **101**, 107006 (2008).
  - [15] S.-W. Park, H. Mizoguchi, K. Kodama, S.-i. Shamoto, T. Otomo, S. Matsuishi, T. Kamiya, and H. Hosono, *Inorg. Chem.* **52**, 13363 (2013).
  - [16] D. J. Singh, A. S. Sefat, M. A. McGuire, B. C. Sales, D. Mandrus, L. H. VanBebber, and V. Keppens, *Phys. Rev. B* **79**, 094429 (2009).
  - [17] P. Das, N. S. Sangeetha, G. R. Lindemann, T. W. Heitmann, A. Kreyssig, A. I. Goldman, R. J. McQueeney, D. C. Johnston, and D. Vaknin, *Phys. Rev. B* **96**, 014411 (2017).
  - [18] S. Nandi, Y. Xiao, N. Qureshi, U. B. Paramanik, W. T. Jin, Y. Su, B. Ouladdiaf, Z. Hossain, and T. Brückel, *Phys. Rev. B* **94**, 094411 (2016).
  - [19] E. Brechtel, G. Cordier, and H. Schäfer, *Z. Naturforsch. B* **34**, 777 (1979).
  - [20] N. T. Stetson and S. M. Kauzlarich, *Inorg. Chem.* **30**, 3969 (1991).
  - [21] S. L. Brock and S. M. Kauzlarich, *Inorg. Chem.* **33**, 2491 (1994).
  - [22] S. Brock and S. Kauzlarich, *J. Alloy. Compd.* **241**, 82 (1996).
  - [23] S. Brock, N. Raju, J. Greedan, and S. Kauzlarich, *J. Alloy. Compd.* **237**, 9 (1996).
  - [24] T. Ozawa, M. M. Olmstead, S. L. Brock, S. M. Kauzlarich, and D. M. Young, *Chem. Mater.* **10**, 392 (1998).
  - [25] A. Matsushita, T. C. Ozawa, J. Tang, and S. M. Kauzlarich, *Physica B* **284-288**, 1424 (2000).
  - [26] T. C. Ozawa, S. M. Kauzlarich, M. Bieringer, C. R. Wiebe, J. E. Greedan, and J. S. Gardner, *Chem. Mater.* **13**, 973 (2001).
  - [27] R. Nath, V. O. Garlea, A. I. Goldman, and D. C. Johnston, *Phys. Rev. B* **81**, 224513 (2010).
  - [28] N. Eguchi, F. Ishikawa, M. Kodama, T. Wakabayashi, A. Nakayama, A. Ohmura, and Y. Yamada, *J. Phys. Soc. Jpn.* **82**, 045002 (2013).

- [29] W. J. Zhu, P. H. Hor, A. J. Jacobson, G. Crisci, T. A. Albright, S.-H. Wang, and T. Vogt, *J. Am. Chem. Soc.* **119**, 12398 (1997).
- [30] W. Zhu and P. Hor, *J. Solid State Chem.* **130**, 319 (1997).
- [31] K. Otzsch, H. Ogino, J.-i. Shimoyama, and K. Kishio, *J. Low Temp. Phys.* **117**, 729 (1999).
- [32] Z. A. Gál, O. J. Rutt, C. F. Smura, T. P. Overton, N. Barrier, S. J. Clarke, and J. Hadermann, *J. Am. Chem. Soc.* **128**, 8530 (2006).
- [33] C. F. Smura, D. R. Parker, M. Zbiri, M. R. Johnson, Z. A. Gál, and S. J. Clarke, *J. Am. Chem. Soc.* **133**, 2691 (2011).
- [34] S. Jin, X. Chen, J. Guo, M. Lei, J. Lin, J. Xi, W. Wang, and W. Wang, *Inorg. Chem.* **51**, 10185 (2012).
- [35] L. M. Volkova, *Supercond. Sci. Technol.* **21**, 095019 (2008).
- [36] T. C. Ozawa and S. M. Kauzlarich, *Sci. Technol. Adv. Mater.* **9**, 033003 (2008).
- [37] X. Dai, C.-C. Le, X.-X. Wu, and J.-P. Hu, *Chin. Phys. B* **25**, 077402 (2016).
- [38] H. Jiang, J.-K. Bao, H.-F. Zhai, Z.-T. Tang, Y.-L. Sun, Y. Liu, Z.-C. Wang, H. Bai, Z.-A. Xu, and G.-H. Cao, *Phys. Rev. B* **92**, 205107 (2015).
- [39] R. J. Birgeneau, H. J. Guggenheim, and G. Shirane, *Phys. Rev. B* **1**, 2211 (1970).
- [40] D. Vaknin, S. K. Sinha, D. E. Moncton, D. C. Johnston, J. M. Newsam, C. R. Safinya, and H. E. King, Jr., *Phys. Rev. Lett.* **58**, 2802 (1987).
- [41] V. O. Garlea, B. C. Chakoumakos, S. A. Moore, G. B. Taylor, T. Chae, R. G. Maples, R. A. Riedel, G. W. Lynn, and D. L. Selby, *Appl. Phys. A* **99**, 531 (2010).
- [42] J. Rodríguez-Carvajal, *Physica B* **192**, 55 (1993).
- [43] H. M. Rietveld, *J. Appl. Cryst.* **2**, 65 (1969).
- [44] A. Le Bail, H. Duroy, and J. L. Fourquet, *Mater. Res. Bull.* **23**, 447 (1988).
- [45] H. G. Scott, *J. Appl. Crystallogr.* **16**, 159 (1983).
- [46] M. Sakata, and M. J. Cooper, *J. Appl. Crystallogr.* **12**, 554 (1979).
- [47] C.-H. Lee, A. Iyo, H. Eisaki, H. Kito, M. T. Fernandez-Diaz, T. Ito, K. Kihou, H. Matsuhata, M. Braden, and K. Yamada, *J. Phys. Soc. Jpn.* **77**, 083704 (2008).
- [48] Y. Qiu, W. Bao, Q. Huang, T. Yildirim, J. M. Simmons, M. A. Green, J. W. Lynn, Y. C. Gasparovic, J. Li, T. Wu, G. Wu, and X. H. Chen, *Phys. Rev. Lett.* **101**, 257002 (2008).
- [49] Y. Mizuguchi, Y. Hara, K. Deguchi, S. Tsuda, T. Yamaguchi, K. Takeda, H. Kotegawa, H. Tou, and Y. Takano, *Supercond. Sci. Technol.* **23**, 054013 (2010).
- [50] G. Shirane, *Acta Crystallogr.* **12**, 282 (1959).
- [51] E. F. Bertaut, *Acta Crystallogr. A* **24**, 217 (1968).
- [52] K. A. Filsinger, W. Schnelle, P. Adler, G. H. Fecher, M. Reehuis, A. Hoser, J.-U. Hoffmann, P. Werner, M. Greenblatt, and C. Felser, *Phys. Rev. B* **95**, 184414 (2017).
- [53] M. Enjalran, R. T. Scalettar, and S. M. Kauzlarich, *Phys. Rev. B* **61**, 14570 (2000).